Instrument Science Report WFC3 2009-43

"Snowballs" in the WFC3-IR Channel: Characterization

B. Hilbert
December 03, 2009

ABSTRACT

We have searched WFC3-IR channel data from two different epochs in order to identify and characterize "snowballs". These snowballs are transient, extended sources with unknown origins that appear in FPA165 ground testing data at rates between 0.4 and 0.8 snowballs per hour of exposure time. A snowball affects between 11 and 34 pixels, and contains between 200,000 and 900,000 e-. With their behavior mimicing that of cosmic ray impacts, CALWF3 should be able to remove snowballs from WFC3-IR data. That, combined with snowballs' low rate of occurrence, implies that snowballs should have a minimal impact on science observations.

Introduction

Recently, a new feature was identified in ground testing data for the WFC3-IR channel. These sources have been dubbed "snowballs", due to their extended, fuzzy appearance in the data. These snowballs appeared very infrequently in ground testing, and with a behavior very similar to that seen with cosmic ray hits on the detector. The entire signal of a snowball appears between consecutive reads of the detector, after which the affected pixels return to their normal behavior. (See Figure 1 for an example plot).

Our goal with this study was to identify snowballs in ground testing data, in order to characterize the snowballs' properities. We then produced a catalog which will provide a useful comparison to any snowballs observed on orbit. The information contained in the catalog will also be useful for exploring possible causes of the snowballs, two of which are briefly dicussed here and investigated more fully by McCullough (2009, in press).

Test Setting	Date	Exposure Time per Ramp (min)	Number of Ramps
DCL (FPA165 prior to integration)	24 April 2007	30	8
	26 April 2007	30	10
	27 April 2007	1 sec	9
	28 April 2007	10	9
	29 April 2007	30	43
	1 May 2007	30	12
	11 May 2007	30	14
TV3	11 March, 18 March, 26 March, 15 April, 16 April 2008	0.73 (RAPID)	15
		2.4 (SPARS10)	15
		5.9 (SPARS25)	15
		11.7 (SPARS50)	15
		28.4 (SPARS100)	15
		46.7 (SPARS200)	15
	16 March, 20 March, 26 March, 15 April, 16 April 2008	4.6 (STEP25)	15
		8.3 (STEP50)	15
		15.0 (STEP100)	15
		26.7 (STEP200)	15
		46.7 (STEP400)	15
	16 March, 8 April 2008	10.0 (MIF600)	6
		15.0 (MIF900)	6
		20.0 (MIF1200)	6
		25.0 (MIF1500)	6

Table 1: IR dark current data from FPA165 (the WFC3 flight IR detector) used in the analysis of snowballs. Total exposure time examined is 2700 minutes (45 hours) of DCL data and 3300 minutes (55 hours) of TV3 data.

Data

We searched for snowballs within two epochs of IR detector data. Prior to integration into the WFC3 flight hardware as the flight detector, FPA165 underwent testing in the Data Characterization Lab (DCL) at Goddard Space Flight Center. As part of this testing, many dark current ramps were collected in April and May of 2007. For the purposes of this study, we examined 108 dark current ramps with exposure times between 43 seconds and 30 minutes per ramp.

We also searched for snowballs in a set of dark current ramps collected during Thermal Vacuum 3 (TV3) testing. These ramps included dark current ramps taken as part of the IR01S01, IR01S02 and IR01S03 Science Mission Specifications (SMSs). These SMSs collected full frame dark current data using all of the SPARS, STEP, and MIF sample sequences (Petro and Wheeler, 2006). These ramps had exposure times between 11.7 and 46.7 minutes per ramp and were collected in March and April of 2008, roughly one year after the DCL data were acquired. Details of the dark current data from both datasets are presented in Table 1, while Tables 2 and 3 show the files in which snowballs were identified. As expected, we see that most snowballs were observed in ramps with longer exposure times. The number of snowballs observed was proportional to exposure time. The total exposure times represented in the two datasets are 45 hours for the DCL data, and 55 hours for the TV3 data. FPA temperature was 145K for both datasets.

Analysis

Each dark current ramp was composed of 16 reads of the detector. Prior to analysis, bias signal in each read was removed through subtraction of reference pixel signals. In order to search for snowballs, where the detector registered a large amount of signal in a short amount of time before returning to the nominal dark current rate, we examined images created from the differences of consecutive reads within a ramp. For each 16-read ramp, we created 15 difference images. We then searched each difference image for pixels containing signal more than 50σ above the background signal level. In order to differentiate snowballs from the more common cosmic ray hits, we also examined the 4 nearest neighbors to each high signal pixel. Only if all 4 neighboring pixels had signal levels more than 25σ above the background level was a given event recorded as a snowball. We also checked to be sure that the central pixel did not have an elevated signal in all image differences up the ramp, as this would indicate a high dark current pixel.

The large threshold values used were set with the fore knowledge that snowballs were large events, with saturated pixels and signals much higher than the background level. Figure 1 shows a plot of the measured signal versus time for 8 pixels stretching through the center of a snowball. This snowball was found in a STEP400 ramp taken during ground testing. This plot shows that all 8 pixels in the row measured jumps in flux between the read at the 200 second mark, and that at the 400 second mark. The size of the flux increase changed with distance from the center of the snowball. The three central pixels received more than 20,000 DN each when the snowball appeared. This was enough to drive these pixels into saturation, as exhibited by the flat or decreasing curves after the snowball. These pixels no longer recorded dark current after being affected by the snowball. The other 5 pixles were outside of the core of the snowball and therefore

measured less flux. These pixels measured fluxes of up to several hundred DN related to the snowball. After the snowball appeared, these pixels continued to measure dark current, as seen by the curves increasing with time. This type of behavior, with several saturated core pixels surrounded by lesser affected outer pixels, is common to all snowballs. For every snowball, the entire flux was also observed to arrive between consecutive reads regardless of sample timing, implying that the snowball appeared instantaneously.

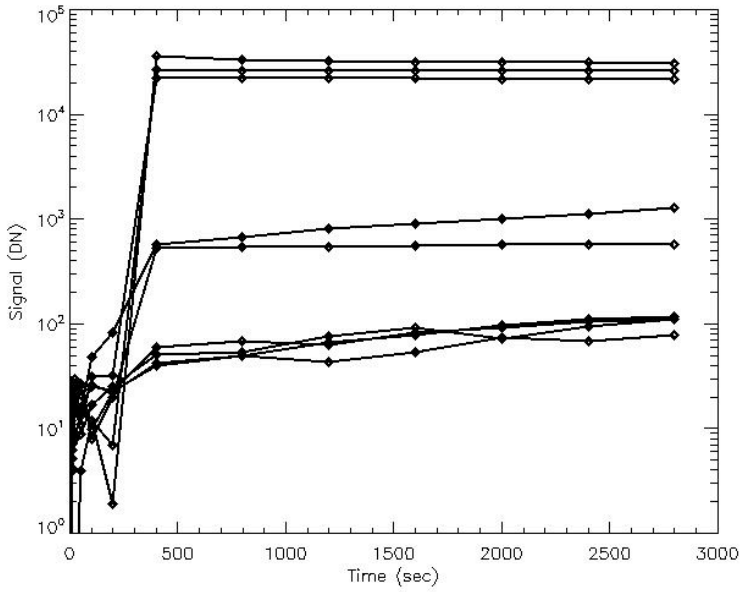

Figure 1: Plot of recorded signal versus time in 8 pixels stretching across the width of a snowball. All snowball-related flux arrived between the two consecutive reads at 200 seconds and 400 seconds, and caused pixels to measure a jump in signal between several tens and several tens of thousands of DN. The three pixels in the center of this row of 8 received enough snowball-associated flux to be at or just below saturation.

By searching through only dark current ramps, we focused on data with low background levels and no other competing light sources. In this case, 25σ above the background level was still very low in terms of absolute signal level. Therefore we're confident that we have not missed any snowballs in the creation of our atlas.

Once a snowball was identified, we collected basic characteristics, including the position of the snowball on the detector, the total flux, the number of pixels effected, the number of saturated pixels, and the time when the event occurred. From this information, we attempted to characterize these snowballs, with an aim towards determining their source, as well as how they might be treated by CALWF3, the standard WFC3 data

reduction software. The full snowball catalogs for both TV3 and DCL data are located in the Appendix. The following sections detail our findings for the two datasets.

DCL Data

Figure 2 shows the location on the detector of the 36 snowball events identified in the DCL data. The snowballs appear to be distrbuted randomly across the detector. This distribution is consistent with the theory of energetic particles as the source of the snowballs. Beginning in the upper left quadrant and traveling around the detector in a counter-clockwise direction, we saw 7, 8, 8, and 13 snowballs in each quadrant. Figure 3 shows a cutout image for each snowball observed in DCL testing. Note that snowballs are always circular. They do not appear enlongated, as can happen with cosmic ray effects.

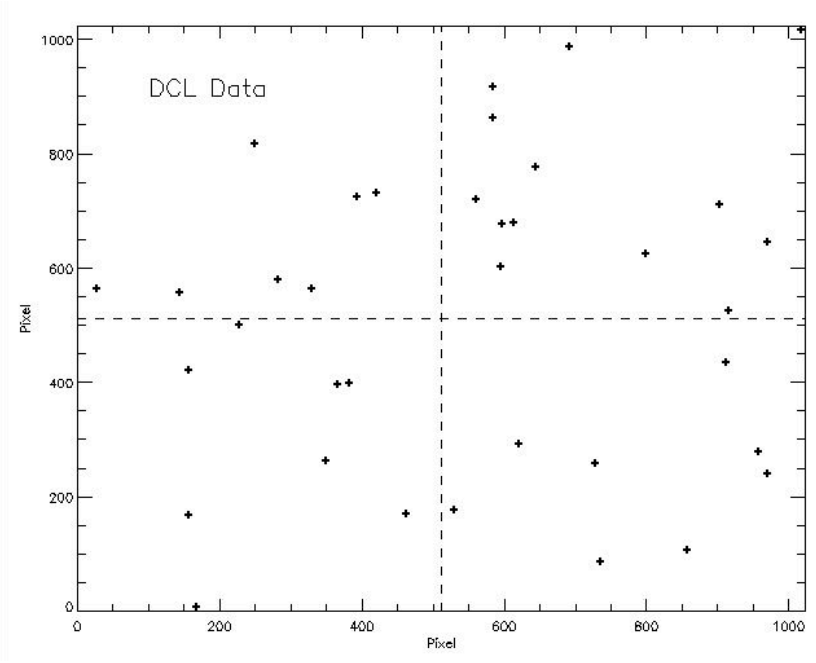

Figure 2: Location of all snowball events identified in the DCL data.

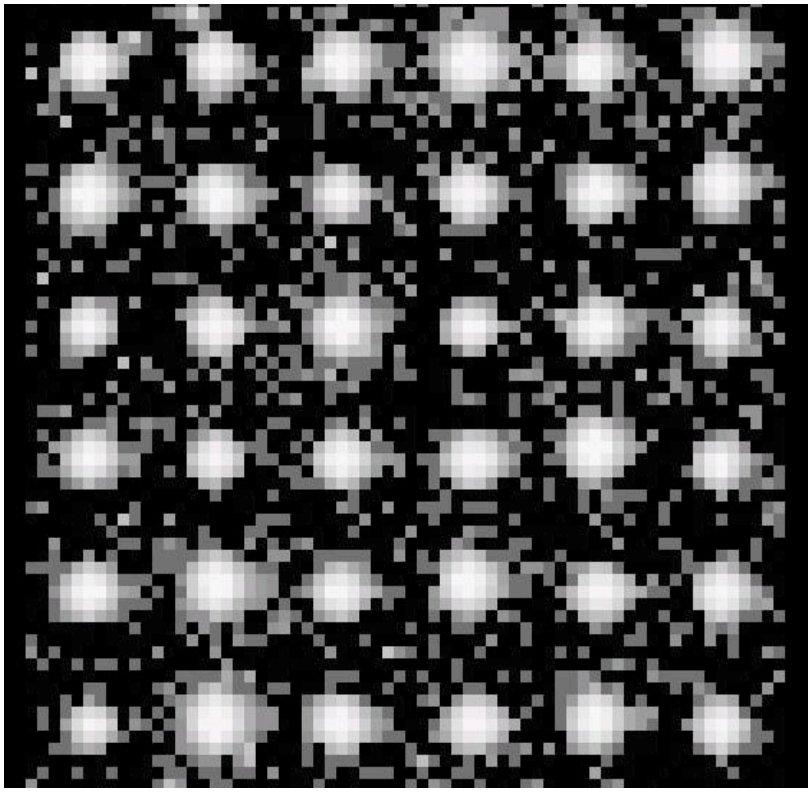

Figure 3: Cutouts of all snowball events identified in the DCL data.

The next snowball characteristic we investigated was the timing of the events. If snowballs are the result of energetic particles impinging the detector or radioactive decay within the detector material, we would expect to see snowballs distributed randomly throughout the testing. Figure 4 shows a timeline of the DCL observations. Each of the 7 panels represents a 12 hour block of time. The blue line indicates time during which data were being collected, and the red diamonds show the times at which snowballs were observed. The snowballs appear randomly distributed throughout the DCL test.

Figure 5 shows a histogram of the time between snowball arrivals during the DCL test. For this histogram, we included only inter-arrival times where observations were made continuously between snowballs. We did not include any data where there was a break in observations between one snowball and the next due to the fact that we could have missed the appearance of a snowball while observations were stopped.

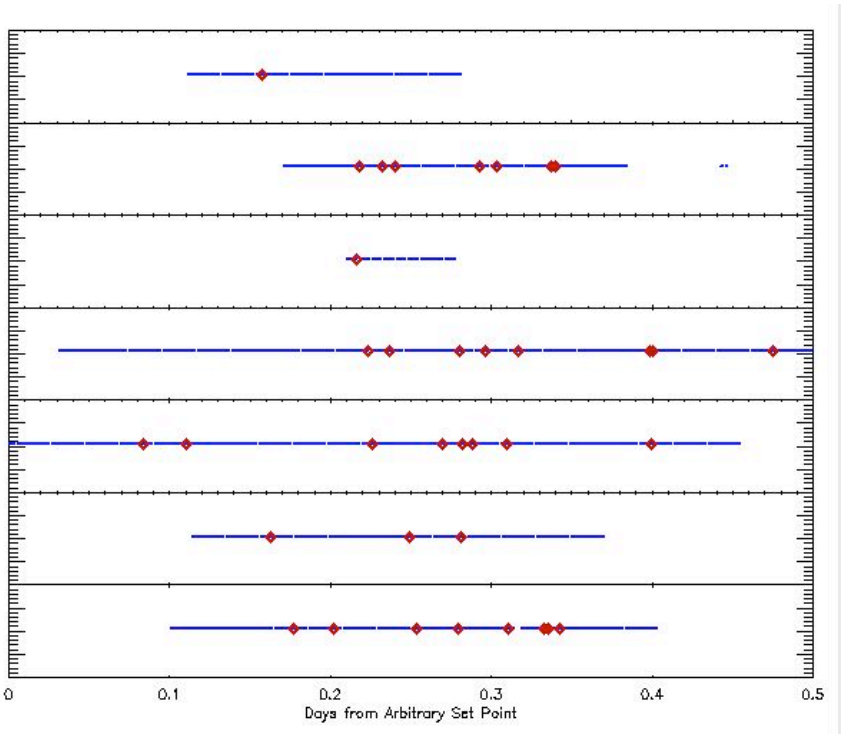

Figure 4: Seven 12-hour periods in the DCL. Blue lines represent time when observations were being made, and red diamonds indicate times when snowballs were observed.

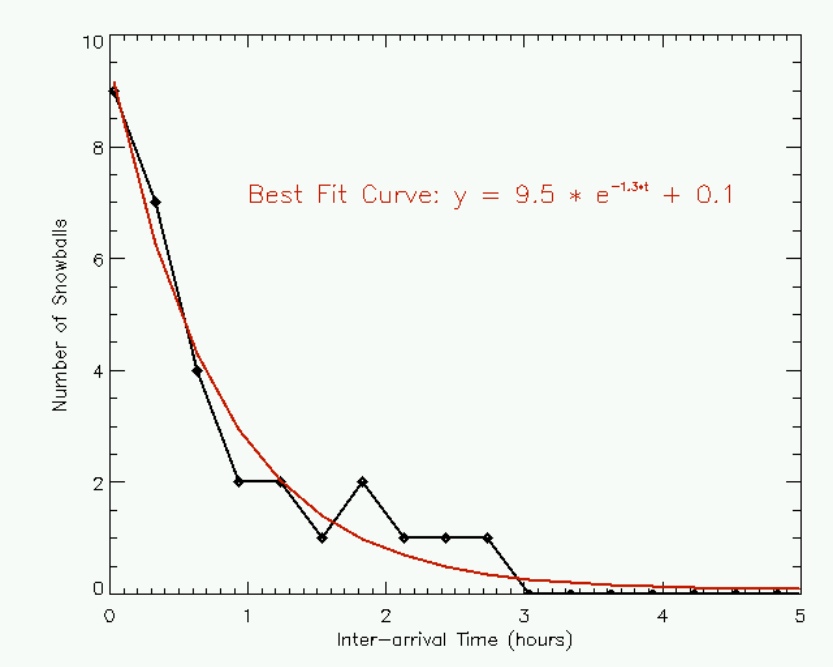

Figure 5: Histogram of the times between snowball arrivals, from the data presented in Figure 4. This histogram includes only the inter-arrival times between snowballs where observations were made continuously between the snowballs. The best-fit exponential curve to this histogram has a decay constant of -1.3.

The overall snowball rate in the DCL data, including all files, is 0.8 snowballs per hour of observing time. The largest continuous subset of data during the testing is shown in the 4th and 5th panels from the top of Figure 4. These panels represent the data from April 29th. Looking at only this subset of data, we see 16 snowballs over 21.5 hours of observation time. This is a rate of 0.74 snowball per hour, matching that of the entire data set.

Next, we examined the spatial area affected by the snowballs in the DCL data. Figure 6 shows a histogram of the total area, in pixels, of the snowballs observed in the DCL data. In this case, a pixel is determined to have been affected if its signal is more than 5σ above the measured background. There is a clear peak in the histogram at an area of 21 pixels.

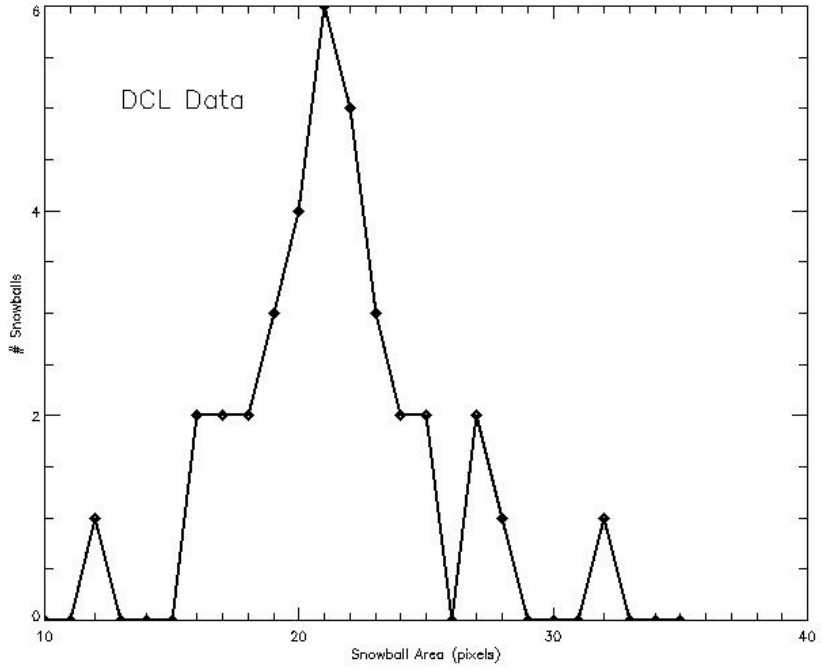

Figure 6: Total area (in pixels) affected by snowballs in the DCL data.

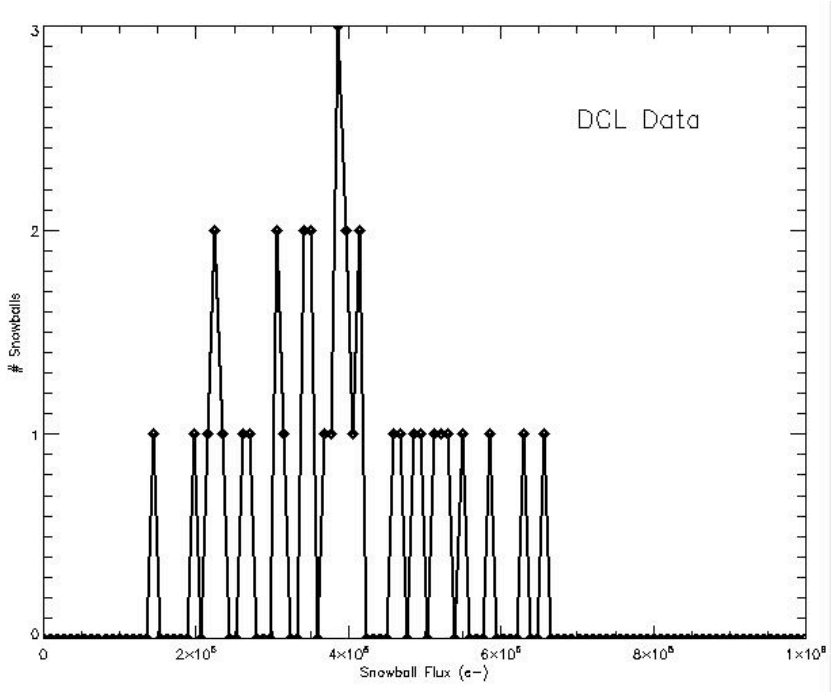

Figure 7: Histogram of the total signal measured by the detector in the DCL snowballs.

Figure 7 shows a histogram of the total flux deposited in the snowball. This histogram is much more flat than that of the snowball area, with measured signals between 200,000 and 600,000 e-. Signals between 300,000 and 400,000 e- are slightly more common than the rest.

One characteristic all snowballs share is that the central few pixels are saturated. Figure 8 is a histogram of the number of saturated pixels in each snowball. As expected, snowballs with fewer saturated pixels also fall on the lower end of the flux histogram, while those with more saturated pixels have a higher total flux. No snowballs with less than 3 saturated pixels had a total flux above the peak at 400,000 e-. Note that since each snowball contains saturated pixels, these flux values are lower limits. Unlike CCD detectors, any signal above the saturation level in a HgCdTe pixel does not bleed into adjacent pixels and get collected.

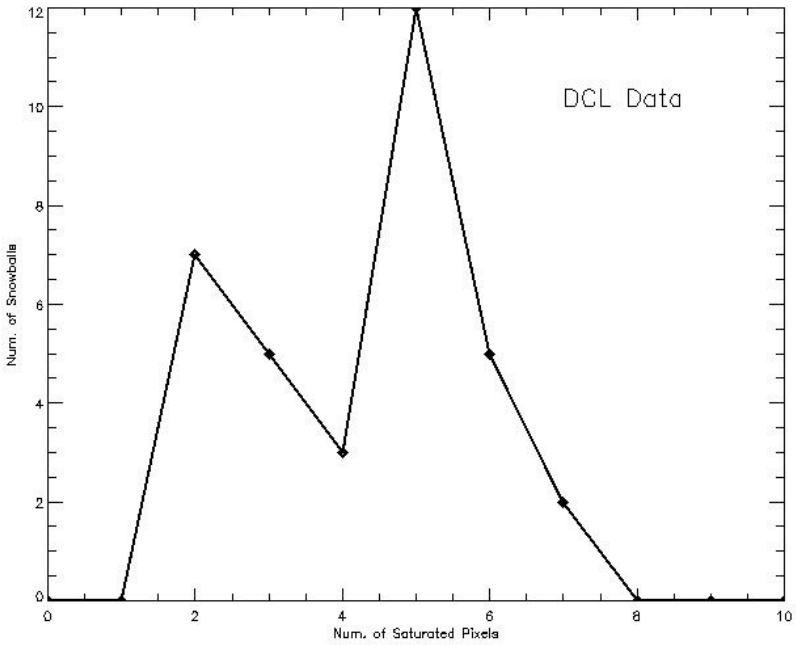

Figure 8: Histogram of the number of saturated pixels in DCL data snowballs.

The final snowball characteristic which we invesetigated was perhaps the most interesting. We found that the positions of observed snowballs on the detector were corellated with previously-defined "unstable pixels". See Hilbert (2007) for a more detailed description of unstable pixels. These pixels were observed to have an unrepeatable reponse during a set of nominally identical ramps, or saturation levels that varied from ramp to ramp. These pixels were declared uncalabratable, and flagged in data quality arrays as pixels to be avoided in future analyses.

Of the 36 snowballs identified in the DCL data, we found that all snowballs had at least one pixel previously flagged as unstable within a 20x20 pixel box. Fifteen of the 36 snowballs had at least one unstable pixel located within the snowball's area, and 4 snowballs had an unstable pixel in the core (ie saturated area) of the snowball.

In order to understand if these observations are statistically significant, we created a control case. Beginning with the mask of unstable pixels, we moved pixel-by-pixel through the detector. For each pixel, we noted the number of unstable pixels within a 20x20 pixel box as well as a 6x6 pixel box. From this, we were able to calculate the probability that a randomly placed snowball would have at least N unstable pixels nearby (20x20 pixel box) or within the snowball itself (6x6 pixel box). Figure 9 shows the results of these calculations.

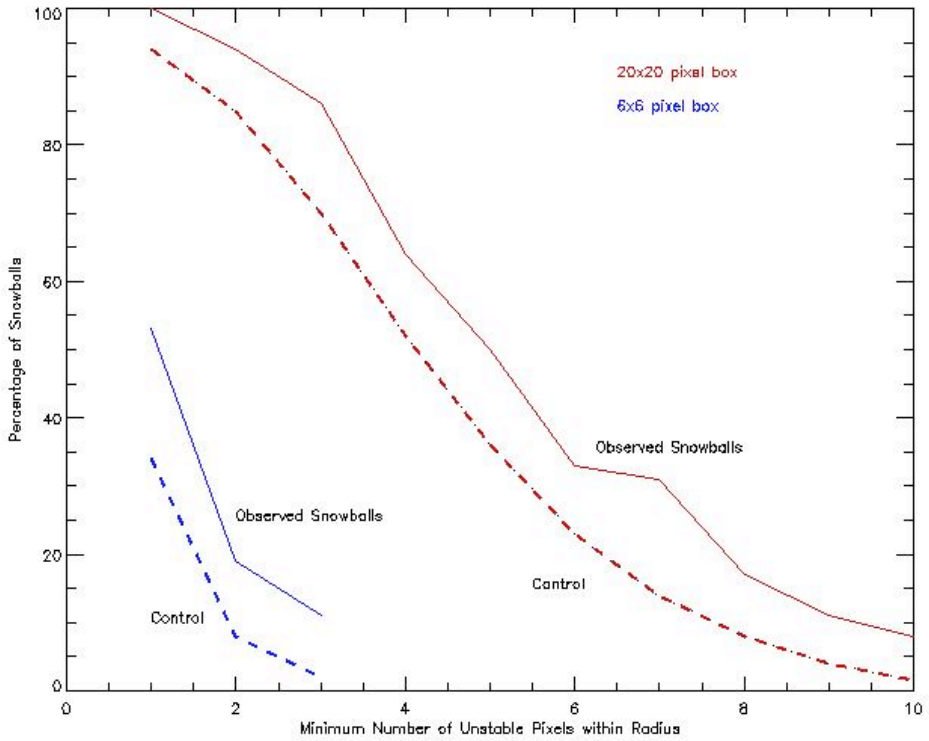

Figure 9: Probabilities that randomly placed snowballs fall close to N or more unstable pixels, along with the percentage of observed snowballs close to unstable pixels. As an example, looking at the 20x20 pixel box (red curves), we see that if snowballs and unstable pixels are uncorrelated (control case, dashed line), we would expect 50% of all snowballs to have 4 or more unstable pixels within a surrounding 20x20 pixel box. However, we observe (solid line) that ~65% of the snowballs in the DCL data have 4 or more unstable pixels within the 20x20 pixel box.

Here, the red curves correspond to calculations done using a 20x20 pixel box, while the blue curves show the results using the 6x6 pixel box. In the case of unstable pixels in the vicinity of the snowball (20x20 box), the ~10% offset between the control curve and the observations indicate that we observed 10% more snowballs near any number of unstable pixels than expected if snowballs and unstable pixels are uncorrelated.

The discrepancy between observed and the control case increases when looking at the 6x6 pixel box. In that case, up to 20% more snowballs contain unstable pixels than expected if the two are uncorrelated.

TV3 Data

Approximately one year after the DCL data above were collected, the fully integrated IR channel went through thermal vacuum testing at Goddard Space Flight center. Using the dark current data collected as part of this test, we were able to search again for snowballs. The total exposure time for this dataset was ~20% longer than the DCL dataset, but we identified ~40% fewer snowballs. Possible explanations for this are described in the conclusions.

Figure 10 shows the position on the detector for all snowballs identified in the TV3 data. The differences between the diamonds and crosses will be discussed below. As with the DCL data, the snowballs appear to be randomly distributed across the detector. Working counter-clockwise around the detector starting from the upper left quadrant, we found 3, 8, 5 and 5 snowballs per quadrant. No two snowballs fell on the same spot of the detector, and none fell on spots hit during DCL testing.

No snowballs were observed in the reference pixels during ground testing. However, with only 1/50 the area of the science pixels and only 57 snowballs observed between DCL and TV3 testing, we do not necessarily expect to have seen a snowball in the reference pixels yet. Once the source of the snowballs is understood, there may also be a physical reason for them not to appear in the reference pixels.

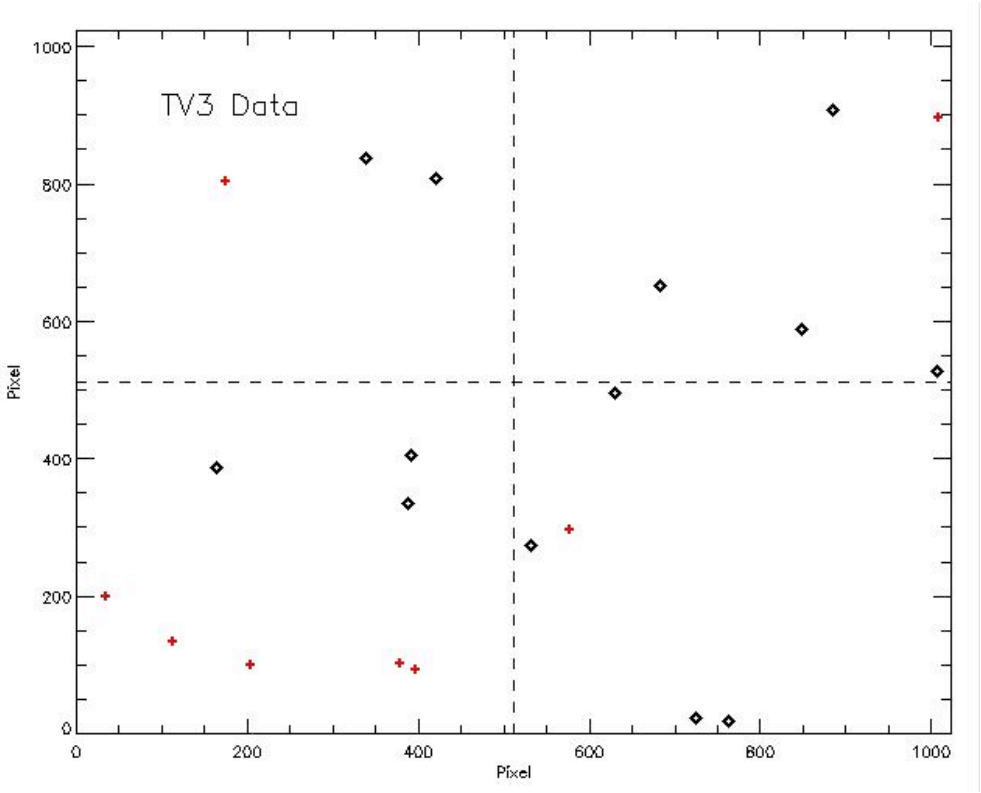

Figure 10: Positions of snowballs observed in TV3 data. Diamonds show lower flux snowballs, while crosses show higher flux snowballs.

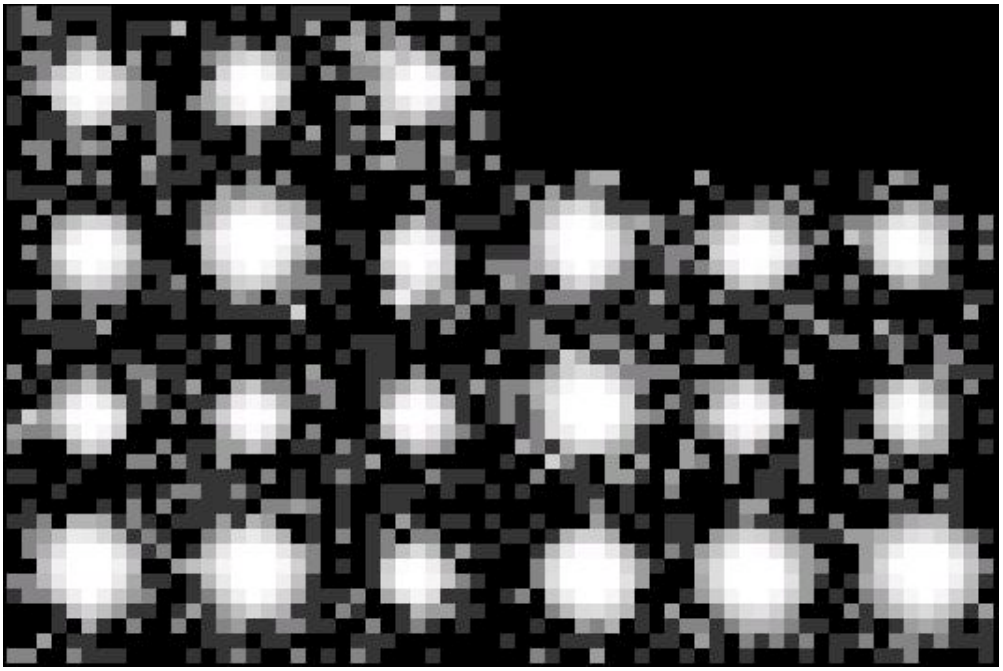

Figure 11: Cutout images of all snowballs identified in TV3 data.

Figure 12 is similar to Figure 4, and shows the timeline of snowball appearances. The scale of this plot is idenitcal to that in Figure 4, with each panel showing a 12 hour block of time. Blue lines represent time during which observations were being made, and red diamonds indicate the presence of a snowball. Totaling up the observations' exposure time, we find snowballs appearing in the TV3 data at a rate of 0.4 snowballs per hour. This is half the observed rate of the DCL data albeit based on small numbers of snowballs. The testing environment is very different between DCL and the thermal vacuum chamber used during TV3. This difference could cause a difference in the observed snowball rate if muons or other high energy particles are the source, but should not affect the snowball rate if radioactive decay is the source.

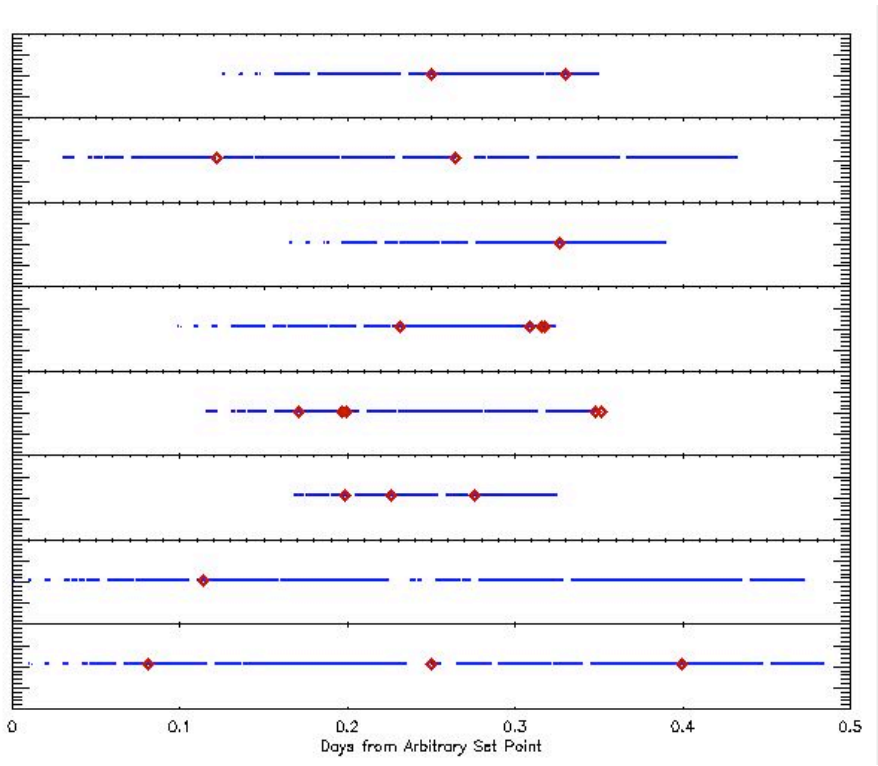

Figure 12: Observation timeline of the TV3 data. Blue lines indicate times when observations were being made, and red diamonds show the times of snowball appearances.

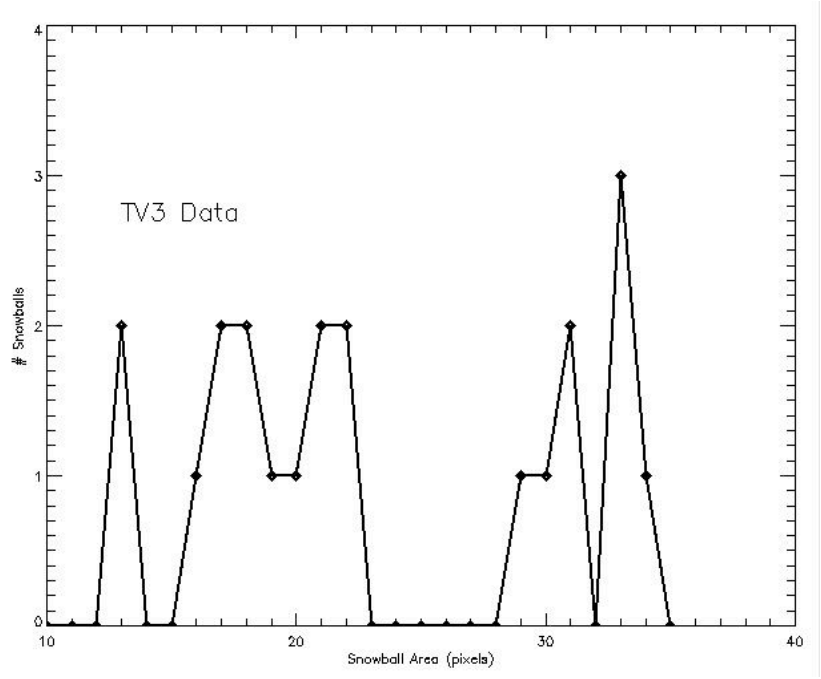

Figure 13: Area in pixels affected by snowballs in TV3.

Similar to the plot shown in Figure 6, Figure 13 shows a histogram of the detector area affected by snowballs in the TV3 data. There are two noticable differences between this histogram and that presented for the DCL data. First, only one snowball in the DCL data affected an area larger than 28 pixels. In contrast, 8 of 21 snowballs in TV3 had areas larger than 28 pixels.

Second, the distribution of DCL snowballs had a clear peak at 21 pixels and then fell steeply above and below this value. In TV3 data however, appears to be bimodal. A relatively flat distribution of snowballs had areas of 16 – 22 pixels, followed by a gap, and a second set of snowballs with areas between 29 and 34 pixels. Looking back at the cutout images in Figure 11, it is easy to see the difference in area between the 8 larger snowballs and the others. Examination of the signal up the ramp in the cases of the larger snowballs reveal that they each is a single snowball, and not two smaller snowballs occuring at the same location with a short delay between them, unless the delay is shorter than the time between reads.

Figure 14, showing the distribution of snowball fluxes, confirms this trend. One group of snowballs had fluxes between 200,000 – 400,00 e-, while a second group had fluxes of 750,000 – 900,000 e-. The largest snowball observed in the DCL data had a flux of approximately 650,000 e-.

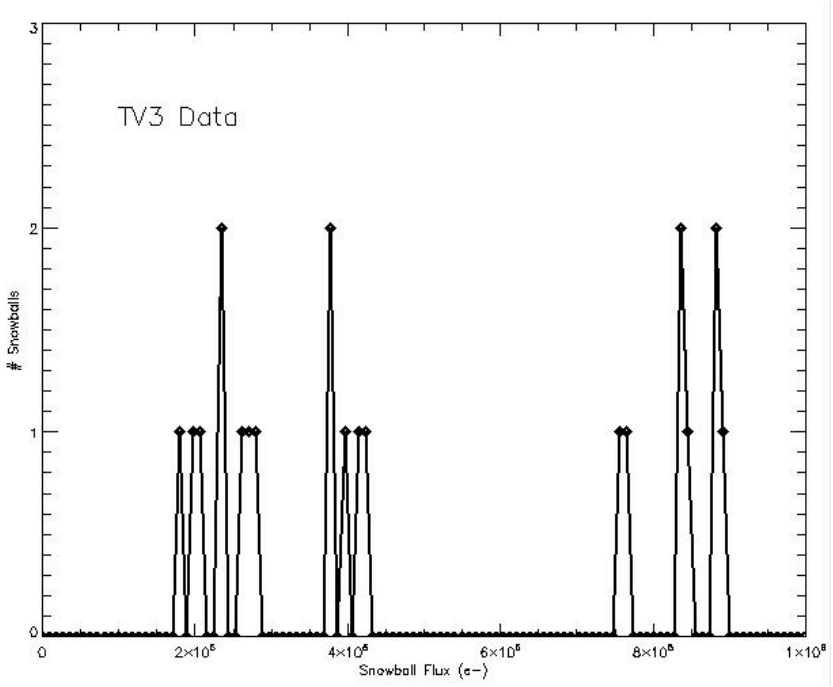

Figure 14: Histogram of the total signal measured by the detector for the group of TV3 snowballs.

Two questions which spring to mind when dicussing larger versus smaller snowalls are: 1) Were the larger snowballs all observed in one part of the detector? 2) Did the large and small snowballs appear as two separate groups in time?

Figure 10, shows the distribution of snowballs across the detector. The crosses indicate the 8 high-flux, large-area snowballs, while the diamonds show the smaller snowballs. Five of the 8 large snowballs were located toward the lower edge of the lower left quadrant of the detector. However, the other three are spread among the other three quadrants. From this it is difficult to make any statements about one area of the detector being prone to higher flux snowballs than others.

Figure 15 addresses the second question from above. This figure shows a plot of the measured flux of the snowballs versus the time at which they occurred. Both high and low signal snowballs were found in each subset of the TV3 data, implying no time-dependence of the low or high flux snowballs.

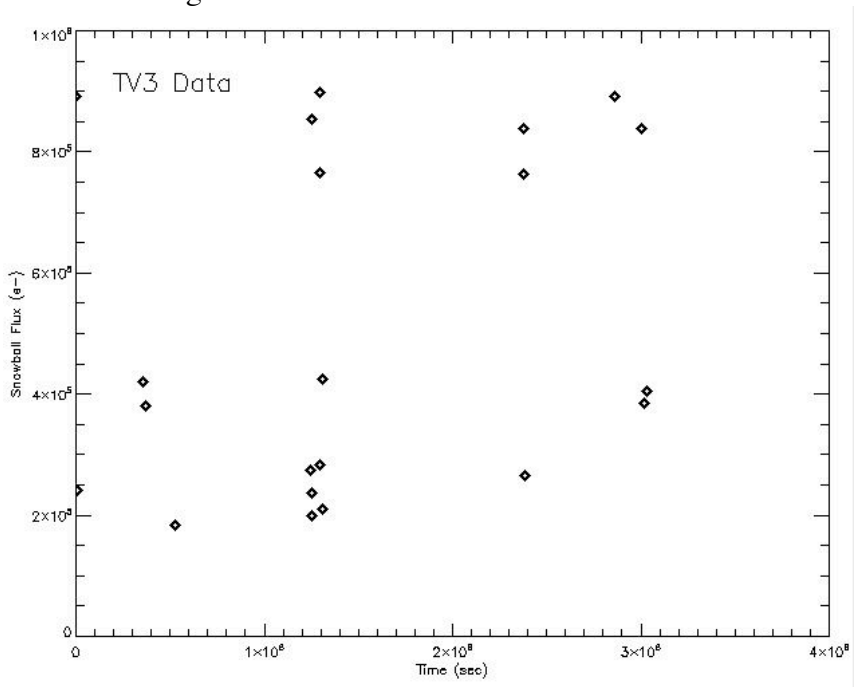

Figure 15: The measured flux of the TV3 snowballs versus the time observed. High and low flux snowballs were observed throughout TV3 testing.

As with the DCL data, Figure 16 shows a histogram of the number of saturated pixels in all TV3 snowballs, similar to that seen in Figure 8. As with the pixel area and flux histograms, we see that a significant number of TV3 snowballs saturated more pixels than the 8 pixels saturated in the largest DCL snowball.

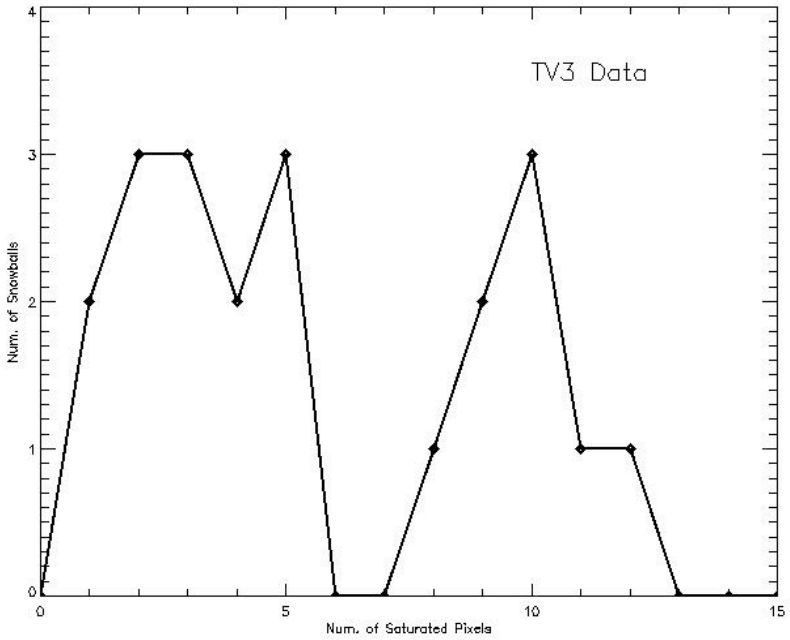

Figure 16: Histogram of the number of saturated pixels in TV3 snowballs.

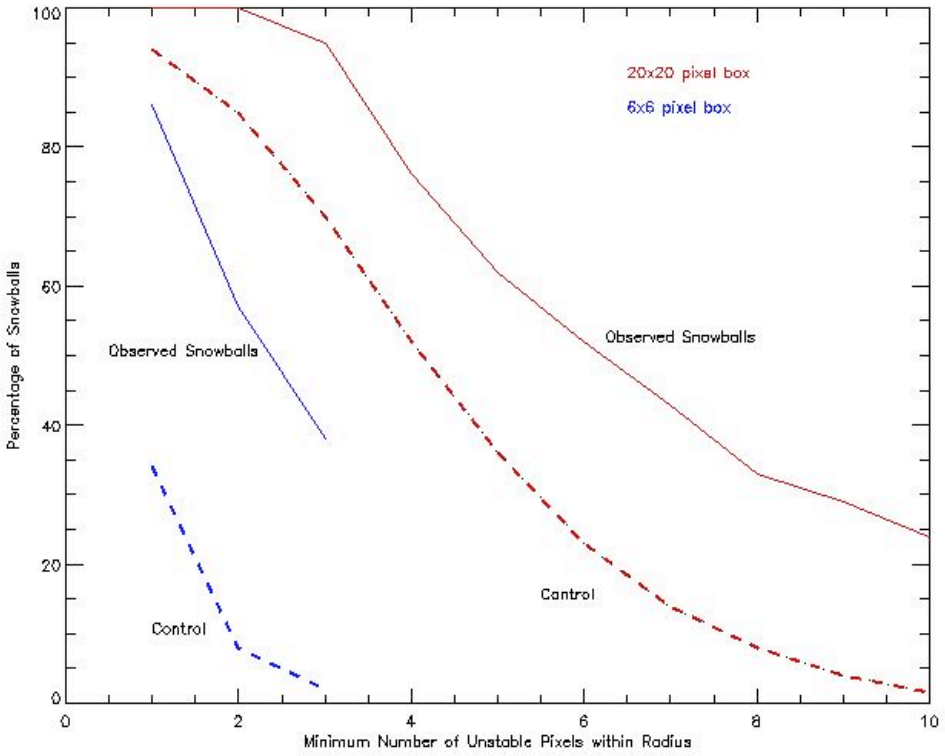

Figure 17: same as Figure 9, for TV3 data. The differences between the observed snowballs and the case of uncorellated snowballs/unstable pixels (control case) is even larger than in the DCL data.

Finally, similar to Figure 9, we look at the percentage of observed snowballs which are coincident with previously defined unstable pixels. For a 20x20 pixel box around snowballs (red curves), we see roughly 15 - 20% more snowballs with unstable pixels close to them than we'd expect for uncorellated snowballs and unstable pixels. In the case of unstable pixels falling within snowballs (blue curves), we see an even larger difference. In the control, we see that roughly 35% of snowballs randomly placed on the detector should have 1 or more unstable pixels within the area of the snowballs. But in the TV3 data, more than 85% of the snowballs fell on top of at least 1 unstable pixel. Similarly, just under 40% of TV3 snowballs fell on top of 3 or more unstable pixels. In the case of uncorellated snowballs and unstable pixels, we'd expect to see less than 5% of all snowballs in this situation.

One of the most compelling cases arguing for a realtion between unstable pixels and snowballs is shown in Figure 18. Here the snowball, along with several nearby hot pixels, is shown in white. The red pixels overlaying the image are pixels previously marked as unstable. Seven pixels making up the core of the snowball are unstable, as well as a group pixels surrounding the snowball (all of which were identified as unstable prior to the discovery of snowballs). Also notable are two pixels on the right side of the snowball (identifiable by the increased signal in the 4 neighboring pixels around each) which had high signal in the image (~16,000 and ~20,000DN for the upper and lower pixels). These pixels also correspond to previously identified unstable pixels.

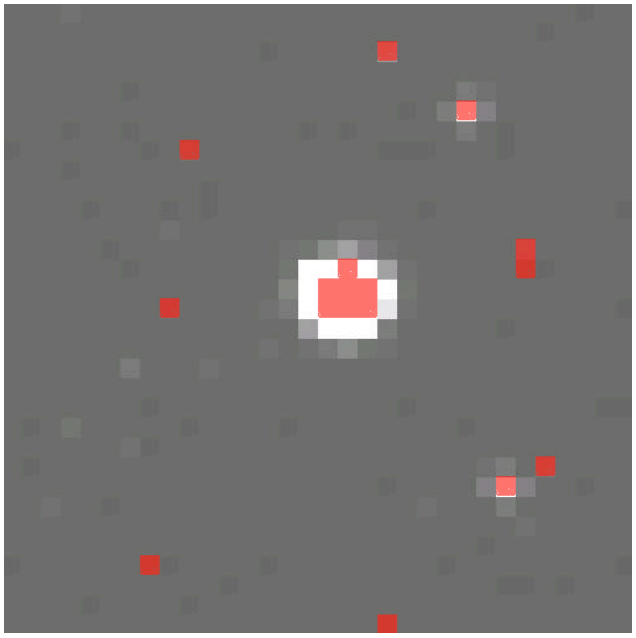

Figure 18: Image of one of the snowballs from TV3. The greyscale portion shows the signal in the snowball and surrounding area. Higher signal is lighter. Overlain red pixels mark previously defined unstable pixels. In addition to the majority of core of the snowball, the two hot pixels to the right of the snowball (each surrounded by a cross of pixels with above-background signals, due to intra-pixel capacitance) are also unstable.

Possible Causes

With the small number of snowballs observed by the WFC3-IR channel, there is still uncertainty as to the ultimate source of the snowballs. Here we briefly present two possibilities. Once we have on-orbit data to supplement the ground test data, we may be in a better position to identify the true source.

One potential source of the snowballs is muon interactions with the detector material. The random scatter of snowballs in space and time, as shown in Figures 2, 4, 10 and 12, is consistent with energetic particles as the source of snowballs. According to the Lawrence Berkeley National Laboratory's Cosmic Ray Telescope Project (Kliewer et al), typical muon flux at sea level is one particle per square centimeter per minute, which is three orders of magnitude higher than the observed snowball rate (0.002 – 0.004 snowballs per cm^2 per minute, assuming an area of 3.33 cm^2 for the IR detector). Different levels of detector shielding between the laboratory setup at DCL and the thermal vacuum chamber decreased the flux of incoming muons by unknown amounts during ground testing. As a result, we can only state that we cannot rule out muons as a source of snowballs in the IR detector.

Another theory for snowball production is the decay of radionuclides within the detector material itself. This method has been proposed by others (ie Finger et al., 2008) to explain their snowball-like sources. In our case, the scatter of snowballs across the detector area and ground test time periods again is consistent with radioactive decay of nuclei. McCullough (2009, in press) has performed a more detailed analysis of this possibility.

Data Reduction Implications

CALWF3 (detailed in Kim Quijano, 2009, section 2.3) is the data reduction pipeline for WFC3 and contains an algorithm for removing the effects of cosmic rays in IR channel data. This procedure identifies cosmic rays by searching individual pixels for large signal jumps between adjacent reads in a ramp. The similarity between these signal jumps and those exhibited by the observed snowballs suggests that the cosmic ray rejection algorithm in CALWF3 should be effective at identifying and removing snowballs from IR data.

A preliminary check using the snowballs identified in the TV3 data shows that using the latest cosmic ray rejection parameters, CALWF3 is unable to completely remove the observed snowballs. In all cases, the final output (flt file) from CALWF3 shows anomalous signal in the snowball's location. In most cases CALWF3 appears to have over-corrected, and left behind a large negative signal in the output file. In addition, there is usually also a ring of high signal pixels surrounding the negative core. However, in several cases CALWF3 appears to have under-corrected for the snowball, leaving behind a large portion of the snowball's flux.

CALWF3 also marked the presence of the snowballs in the error array of the final output image. Error values in the pixels affected by a snowball are higher than those in the surrounding background by up to 50%. Curiously, despite these effects on the pixels' signals, CALWF3 failed to mark any of the pixels as impacted by cosmic rays.

Given these results, the parameters in the CALWF3 cosmic ray rejection algorithm will have to be adjusted in order to more effectively identify and remove snowballs. Once we have a collection of on-orbit data, which will contain snowballs as well as many more cosmic rays than were seen in the ground data, we should be able to optimize CALWF3's ability to remove snowballs from IR channel data.

Conclusions

We have created an atlas and performed a basic characterization of the observed snowballs in the IR channel of WFC3. Data taken at the DCL, as well as during TV3 testing show that snowballs appear on the 3.33 cm^2 IR detector at a rate of between 0.4 and 0.8 snowballs per hour. Each snowball affects between 15 and 35 pixels, saturating between 1 and 13 central pixels. The total measured signal of the snowballs ranges from 200,000 to 900,000 e-.

If the snowballs are caused by energetic particles interacting with the material in the IR detector, then we should continue to see snowballs, but at a different rate, in data collected on-orbit.

If instead the decay of radionuclides within the detector material is the cause of the snowballs, we should continue to see snowballs at approximately the same rate as seen during ground testing. Planned SMOV and Cycle 17 dark current monitoring programs will provide a large amount of exposure time to collect more snowball statistics.

References

Finger, G., Dorn, R. J., Eschbaumer, S., Hall, D. N. B., Mehrgan, L., Meyer, M., & Stegmeier, J. 2008, Performance evaluation, readout modes and calibration techniques of HgCdTe HAWAII-2RG mosaic arrays, Proc. SPIE, 7021

Hilbert, B., 2007, WFC3 ISR 2007-25. "**WFC3 TV2 Testing: IR Channel Non-linearity Correction and Unstable Pixel Masking**" 1 Nov 2007.

Hilbert, B., 2008, WFC3 ISR 2008-50. "**WFC3 TV3 Testing: IR Gain Results**" 16 Dec 2008.

Kim Quijano, J., et al. 2009, "WFC3 Mini-Data Handbook", Version 1.0, (Baltimore: STScI)

Kliewer, S. Lawrence Berkeley National Laboratory Cosmic Ray Telescope Project. http://cosmic.lbl.gov/SKliewer/Cosmic_Rays/Muons.htm

McCullough, P. 2009, in press. "**Radioactivity in HgCdTe devices: potential source of 'snowballs'**".

Petro, L. and T. Wheeler, 2006, "**New IR Detector Sample Times**" 2 Oct 2006

Appendix

The following tables list the snowballs discovered in DCL and TV3 ground test data. The fluxes listed are in units of electrons, after applying gain values calculated from TV3 data (Hilbert, 2008). The X and Y values represent the central pixel of the snowball, and include reference pixels. In this case, the science pixels run from (X,Y) = (5,5) in the lower left corner of the detector to (X,Y) = (1018,1018) in the upper right corner. Pixel numbers and read numbers are zero indexed.

DCL snowballs:

Filename	Index	Flux (e-)	Saturated Pixels	Total Pixels	Time(julday)	X	Y	Read
ap24_dk145_30m_0011.fits	0	150149.	2	12	2454215.907737	529	177	3
ap26_dk145_30m_0013.fits	1	664471.	7	32	2454217.817795	143	556	3
ap26_dk145_30m_0013.fits	2	419504.	6	21	2454217.832118	462	169	14
ap26_dk145_30m_0014.fits	3	346080.	4	23	2454217.840567	613	679	4
ap26_dk145_30m_0016.fits	4	396012.	5	22	2454217.892633	957	279	11
ap26_dk145_30m_0017.fits	5	275713.	3	18	2454217.903698	249	818	3
ap26_dk145_30m_0018.fits	6	412879.	5	21	2454217.936887	585	862	12
ap26_dk145_30m_0018.fits	7	556592.	6	27	2454217.939491	365	397	14
ap28_dk145_10min_0001.fits	8	307844.	3	22	2454219.315943	971	645	13
ap29_dk145_30min_0007.fits	9	528784.	6	22	2454220.423084	156	420	15
ap29_dk145_30min_0008.fits	10	316188.	2	20	2454220.436800	27	563	9
ap29_dk145_30min_0010.fits	11	394435.	5	21	2454220.479855	970	240	9
ap29_dk145_30min_0011.fits	12	311668.	3	20	2454220.496186	394	724	5
ap29_dk145_30min_0012.fits	13	221768.	2	18	2454220.516412	597	676	4
ap29_dk145_30min_0016.fits	14	416748.	5	21	2454220.598663	157	168	1
ap29_dk145_30min_0016.fits	15	356699.	3	20	2454220.599965	691	987	2
ap29_dk145_30min_0019.fits	16	586139.	5	25	2454220.675012	168	7	10
ap29_dk145_30min_0024.fits	17	269061.	3	16	2454220.783756	728	257	11
ap29_dk145_30min_0025.fits	18	204332.	2	19	2454220.810446	585	917	15
ap29_dk145_30min_0031.fits	19	344322.	5	21	2454220.926372	383	399	5
ap29_dk145_30min_0033.fits	20	533613.	5	24	2454220.969369	329	563	5
ap29_dk145_30min_0033.fits	21	236687.	2	16	2454220.982390	857	107	15
ap29_dk145_30min_0034.fits	22	383307.	5	23	2454220.988258	596	601	3
ap29_dk145_30min_0035.fits	23	230956.	2	17	2454221.009763	644	776	3
ap29_dk145_30min_0039.fits	24	502964.	5	23	2454221.099722	621	293	6
my01_dk145_30m_0007.fits	25	391941.	4	19	2454222.762946	421	731	5
my01_dk145_30m_0011.fits	26	225083.	2	17	2454222.848895	283	580	5
my01_dk145_30m_0012.fits	27	358739.	5	21	2454222.880804	903	710	13
my11_dk145_30m_0004.fits	28	390507.	5	20	2454232.626846	916	524	9
my11_dk145_30m_0005.fits	29	461240.	6	22	2454232.652245	736	85	12
my11_dk145_30m_0008.fits	30	473758.	4	25	2454232.703669	1018	1016	2
my11_dk145_30m_0009.fits	31	374235.	5	24	2454232.729045	228	501	5
my11_dk145_30m_0010.fits	32	492756.	5	22	2454232.760920	912	434	13
my11_dk145_30m_0016.fits	33	635965.	7	27	2454232.783015	350	262	11
my11_dk145_30m_0016.fits	34	401030.	4	19	2454232.785619	800	624	13
my11_dk145_30m_0017.fits	35	518988.	6	28	2454232.792766	561	720	2

TV3 snowballs:

Filename	Index	Flux (e-)	Saturated Pixels	Total Pixels	Time(julday)	X	Y	Read
ii01030nr_08071233443_raw.fits	0	890534.	10	34	2454537.471504	203	100	10
ii01030tr_08072013842_raw.fits	1	241701.	2	17	2454537.551782	1006	527	8
ii01040fr_08076022853_raw.fits	2	420855.	4	21	2454541.592989	163	388	10
ii01040sr_08076062350_raw.fits	3	381456.	5	21	2454541.735361	388	334	8
ii01030rr_08078030135_raw.fits	4	184262.	1	13	2454543.597754	725	22	13
ii01030nr_08086083242_raw.fits	5	275342.	3	16	2454551.853205	683	652	3
ii01030tr_08086103641_raw.fits	6	236196.	2	18	2454551.930011	884	908	6
ii01030tr_08086103641_raw.fits	7	199616.	1	13	2454551.936955	421	809	3
ii01030tr_08086103641_raw.fits	8	854359.	12	33	2454551.939270	396	93	2
ii010407r_08086224304_raw.fits	9	898302.	9	33	2454552.441959	174	803	8
ii01040dr_08086232830_raw.fits	10	765826.	8	29	2454552.468290	112	133	9
ii01040dr_08086232830_raw.fits	11	284189.	2	19	2454552.470605	848	589	7
ii01040sr_08087033848_raw.fits	12	209453.	3	18	2454552.619598	338	838	9
ii01040sr_08087033848_raw.fits	13	425407.	5	22	2454552.623070	762	18	7
ii010501r_08099112449_raw.fits	14	762890.	9	30	2454564.969659	577	296	9
ii010506r_08099120117_raw.fits	15	839539.	10	31	2454564.997690	378	102	7
ii01050er_08099131846_raw.fits	16	266468.	3	17	2454565.047251	531	273	8
ii01030lr_08105020957_raw.fits	17	890915.	11	33	2454570.585057	34	199	5
ii01030dr_08106180657_raw.fits	18	839252.	10	31	2454572.252534	1008	897	7
ii01030vr_08106222829_raw.fits	19	384631.	5	22	2454572.421469	392	404	7
ii01040lr_08107015956_raw.fits	20	404332.	4	20	2454572.571137	630	496	6